The Astronomical Journal, 163:77 (15pp), 2022 February https://doi.org/10.3847/1538-3881/ac416d

The Transit Timing and Atmosphere of Hot Jupiter HAT-P-37b

Napaporn A-thano[1], Ing-Guey Jiang[1], Supachai Awiphan[2], Ronnakrit Rattanamala[3,4], Li-Hsin Su[1], Torik Hengpiya[5], Devesh P. Sariya[1], Li-Chin Yeh[6], A. A. Shlyapnikov[7], Mark A. Gorbachev[7], Alexey N. Rublevski[7], Vineet Kumar Mannaday[8], Parijat Thakur[8], D. K. Sahu[9], David Mkrtichian[2], and Evgeny Griv[10]
[1] Department of Physics and Institute of Astronomy, National Tsing-Hua University, Hsinchu 30013, Taiwan; napaporn@gapp.nthu.edu.tw, jiang@phys.nthu.edu.tw
[2] National Astronomical Research Institute of Thailand, 260 Moo 4, Donkaew, Mae Rim, Chiang Mai, 50180, Thailand; supachai@narit.or.th
[3] PhD Program in Astronomy, Department of Physics and Materials Science, Faculty of Science, Chiang Mai University, Chiang Mai, 50200, Thailand
[4] Department of Physics and General Science, Faculty of Science and Technology, Nakhon Ratchasima Rajabhat University, Nakhon Ratchasima, 30000, Thailand
[5] Regional Observatory for the Public, Songkhla, 79/4 Moo 4, Khao Roop Chang, Muang District, Songkhla, 90000, Thailand
[6] Institute of Computational and Modeling Science, National Tsing-Hua University, Hsinchu 30013, Taiwan
[7] Crimean Astrophysical Observatory, 298409, Nauchny, Crimea
[8] Department of Pure and Applied Physics, Guru Ghasidas Vishwavidyalaya (A Central University), Bilaspur (C.G.)–495009, India
[9] Indian Institute of Astrophysics, Bangalore–560034, India
[10] Department of Physics, Ben-Gurion University, Beer-Sheva 84105, Israel
Received 2021 September 7; revised 2021 November 11; accepted 2021 November 30; published 2022 January 20

Abstract

We perform transit timing variation (TTV) and transmission spectroscopy analyses of the planet HAT-P-37b, which is a hot Jupiter orbiting a G-type star. Nine new transit light curves are obtained and analyzed together with 21 published light curves from the literature. The updated physical parameters of HAT-P-37b are presented. The TTV analyses show a possibility that the system has an additional planet that induced the TTVs amplitude signal of 1.74 ± 0.17 minutes. If the body is located near the 1:2 mean-motion resonance orbit, the sinusoidal TTV signal could be caused by the gravitational interaction of a sub-Earth-mass planet with mass of 0.06 $M_{\oplus}$. From the analysis of an upper-mass limit for the second planet, a Saturn-mass planet with orbital period less than 6 days is excluded. The broadband transmission spectra of HAT-P-37b favors a cloudy atmospheric model with an outlier spectrum in the *B* filter.

Unified Astronomy Thesaurus concepts: Exoplanet astronomy (486); Exoplanet atmospheres (487)

Supporting material: machine-readable table

1. Introduction

Discoveries of new extrasolar planets through the transit method have grown dramatically in recent years. More than 3000 planets[11] have been confirmed by the transit method. Since the launch of the Kepler space telescope in 2009, more than 2600 planets have discovered using Kepler data (Borucki et al. 2010). After the Kepler era, the majority of exoplanet detection using the transit method has been developed by the Transiting Exoplanet Survey Satellite (TESS; Ricker et al. 2014). To date, more than 140 planets have been confirmed by the TESS mission. Transit light curves can be used to search for additional planets in a planetary system via transit timing variations (TTVs; Agol et al. 2005; Holman & Murray 2005; Maciejewski et al. 2010; Jiang et al. 2013). Additionally, the TTV signal can be used to examine the theoretical predictions of orbital period changes, orbital decay, and apsidal precession (see Maciejewski et al. 2016; Patra et al. 2017; Southworth et al. 2019; Mannaday et al. 2020).

In addition to the discovery of new exoplanets and investigating planetary dynamics, the characterization of planetary interiors and atmospheres is a rapidly developing area. One method that is used to study planetary atmospheres is transmission spectroscopy, which measures the variation of transit depth with wavelength (Seager & Sasselov 2000). The technique has been proven to be one of the most powerful techniques to characterize planet atmospheres. The first planet atmosphere modeling was provided by Seager & Sasselov (2000). The first high-precision spectro-photometric observations of HD 209458 with the Hubble Space Telescope (HST) through absorption from sodium in the planetary atmosphere was reported by Charbonneau et al. (2002). Sing et al. (2016) performed a comparative study of 10 hot Jupiters' atmospheres using transmission spectroscopy. They found that the difference between the planetary radius measured at optical and infrared wavelengths can be applied to distinguish different atmosphere types.

The Hungarian-made Automated Telescope Network (HATNet) is a ground-based telescope network of seven wide-field, small telescopes that monitor bright stars from $r \approx 9$ mag to $r \approx 14$ mag in order to search for new exoplanets via transit method (Bakos et al. 2004)[12] Since the first light in 2003, the HATNet survey has discovered 70 extrasolar planets. A number of hot Jupiters, including HAT-P-58b–HAT-P-60b (Bakos et al. 2021) and HAT-P-35b–HAT-P-37b (Bakos et al. 2012), were discovered by the surveys. In this work, we focus on the photometric follow-up observations of the hot Jupiter HAT-P-37b.

HAT-P-37b, a hot Jupiter orbiting the host G-type star HAT-P-37 ($V = 13.2$, $M_{\star} = 0.929 \pm 0.043 M_{\odot}$, $R_{\star} = 0.877 \pm 0.059 R_{\odot}$, $T_{\rm eff\star} = 5500 \pm 100$ K and $\log_g \star = 4.67 \pm 0.1$ cgs) with a period of 2.8 days, was discovered by Bakos et al. (2012). The existence of HAT-P-37b has been confirmed by radial-velocity measurements from high-resolution

[11] The Extrasolar Planets Encyclopaedia: http://exoplanet.eu/.

[12] The Hungarian-made Automated Telescope Network: https://hatnet.org/.

Table 1
Log of Observations of HAT-P-37b Transits

Observation Date	Epoch	Telescope	Filter	Exposure Time (s)	Number of Images	PNR (%)	Transit Coverage
2014 May 28	416	P60	*R*	30	68	0.24	Ingress only
2014 Jun 11	421	P60	*R*	30	101	0.12	Ingress only
2014 Jul 23	436	P60	*R*	30	160	0.15	Full
2014 Aug 06	441	P60	*R*	30	92	0.14	Ingress only
2017 Apr 02	788	MTM-500	*R*	60	180	0.39	Full
2019 Apr 05	1050	MTM-500	*R*	60	147	0.40	Full
2020 Jul 18	1218	MTM-500	*R*	60	149	0.49	Full
2021 Jul 20	1349	TRT-SRO	*R*	30	405	0.37	Full
2021 Aug 03	1354	TRT-SRO	*B*	90	95	1.25	Egress only

Note. Epoch = 0 is the transit on 2011 March 21. PNR is the photometric noise rate (Fulton et al. 2011).

spectroscopy using the Tillinghast Reflector Echelle Spectrograph and three i'-band follow-up light curves from the KeplerCam instrument. From the data, HAT-P-37b is a Jupiter-mass exoplanet with mass $M_p = 1.169 \pm 0.103 M_{\rm Jup}$, radius $R_p = 1.178 \pm 0.077 R_{\rm Jup}$, and equilibrium temperature $T_{\rm eq} = 1271 \pm 47$ K.

In 2016, HAT-P-37b was revisited by Maciejewski et al. (2016). The obtained planetary parameters modeled from four new transit light curves and published light curves from Bakos et al. (2012) are consistent with the values in Bakos et al. (2012). Turner et al. (2017) presented a photometric follow-up observation by the 1.5 m Kuiper Telescope with the *R* and *B* bands. They derived the physical parameters by combining their two transit light curves and previous public data. They found that the transit depth in the *B* band is smaller than the depth in near-IR bands. The variation may be caused by the TiO/VO absorption in HAT-P-37b's atmosphere. Recently, Yang et al. (2021) performed follow-up photometric observations of HAT-P-37b using the 1 m telescope at Weihai Observatory. The physical and orbital parameters of HAT-P-37b are refined by their new nine light curves combined with previously published data. An investigation of dynamic analysis was presented and there was no significant of TTV signal from the new ephemeris given an rms scatter of 57 s.

In this work, we present new ground-based photometric follow-up observations of nine transit events of HAT-P-37b. These data are combined with available published photometric data in order to constrain the planetary physical parameters, investigate the planetary TTV signal, and constrain the atmospheric model. Our observational data are presented in Section 2. The light-curve analysis is described in Section 3. The study of TTVs includes timing models, frequency analysis, and the upper-mass limit of additional planets, as presented in Section 4. In Section 5, the analysis of HAT-P-37b's atmosphere is given. Finally, the discussion and conclusion are in Section 6.

2. Observational Data

2.1. Observations and Data Reduction

The photometric observations of HAT-P-37b were conducted using the 60 inch telescope (P60) at Palomar Observatory, USA, the 50 cm Maksutov telescope (MTM-500) at the Crimean Astrophysical Observatory, Crimea, and the 0.7 m Thai Robotic Telescope at Sierra Remote Observatories, USA, between 2014 June and 2021 July. Nine transits, including five full transits and four partial transits, in the *R* band and *B* band were obtained. The observation log is given in Table 1.

1. *The 60 inch telescope (P60).* One full transit and three partial transits of HAT-P-37b were obtained by the 60 inch telescope (P60) at Palomar Observatory, California, USA in 2014. The P60 is a reflecting telescope built with Ritchey–Chrétien optics. The field of view of each image is 13×13 arcmin^2, with a 2048×2048 pixel CCD camera.
2. *The 50 cm Maksutov telescope (MTM-500).* During 2017–2020, three full transits of HAT-P-37b were obtained with the 50 cm Maksutov telescope (MTM-500) at the Crimean Astrophysical Observatory (CrAO), Nauchny, Crimea. The observations were performed using an Apogee Alta U6 1024×1024 pixels CCD camera. The field of view is about 12×12 arcmin^2.
3. *0.7 m Thai Robotic Telescope at Sierra Remote Observatories (TRT-SRO).* Recently, one full transit and one partial transit were obtained by the 0.7 m telescope as a part of Thai Robotic Telescope Network operated by National Astronomical Research Institute of Thailand (NARIT). The 0.7 m Robotic Telescope is located at Sierra Remote Observatories (TRT-SRO), California, USA. We observed HAT-P-37b with the Andor iKon-M 934 1024×1024 pixel CCD camara. The field of view was 10×10 arcmin^2.
4. *Data Reduction.* All the science images of HAT-P-37b were calibrated by bias-subtraction, dark-subtraction, and flat corrections using the standard tasks from the `IRAF`[13] package. The astrometic calibration for all science images was performed by `Astrometry.net` (Lang et al. 2010). To create the transit light curve for each observation, the aperture photometry was carried out using `sextractor` (Bertin & Arnouts 1996). The nearby stars from HAT-P-37b with magnitude ± 3 without strong brightness variations were selected to be the reference stars. The time stamps are converted to barycentric Julian date in barycentric dynamical time ($\rm BJD_{TDB}$) using `barycorrpy` (Kanodia & Wright 2018).

[13] IRAF is distributed by the National Optical Astronomy Observatories, which are operated by the Association of Universities for Research in Astronomy, Inc., under cooperative agreement with the National Science Foundation. For more details, see http://iraf.noao.edu/.

2.2. Literature Data

In order to obtain the HAT-P-37b parameters, the 9 transit light curves mentioned in Section 2.1 were combined with 21 published transit light curves. These published light curves include 3 i'-band light curves from Bakos et al. (2012), 4 light curves from Maciejewski et al. (2016; 2 in the Cousins R band, 1 in the Gunn-r band, and 1 with no filter), 2 light curves in Harris B and R filters from Turner et al. (2017), 3 R-band light curves from Wang et al. (2021), and 9 light curves including 7 in V band and 2 in R band from Yang et al. (2021). In total, 30 transit light curves of the HAT-P-37b are used in this work.

Note that we have checked HAT-P-37 data from the Kepler/K2 and TESS databases. HAT-P-37 is not in the Kepler/K2 fields. The planetary system was observed by TESS. However, there is a bright, nearby binary system (<5 TESS pixels). Therefore, the HAT-P-37 TESS light curves are diluted with the flux from that nearby binary and we could not easily detect the HAT-P-37b transit. Therefore, we did not include TESS light curves in this work.

3. Light-curve Analysis

In order to find the best-fit light curves and planetary parameter of HAT-P-37b, we use the `TransitFit`, a python package for fitting multifilter and multiepoch data for exoplanet transit observations, which employs the model transit from `batman` (Kreidberg 2015) and uses the dynamic nested sampling routines from `dynesty` (Speagle 2020) to determine the parameters (Hayes et al. 2021).

All 30 light curves were modeled simultaneously by `TransitFit`. We performed `TransitFit` using the nested sampling algorithm with 2000 live points and 10 sampling slices. Each transit light curve was individually detrended using the second-order polynomial detrending function in `TransitFit` during the retrieval. The normalized light curves with their uncertainties are available in a machine-readable form in Table 2. The initial values of each parameter—orbital period P, epoch of midtransit T_0 (BJD), orbital inclination i (deg), semimajor axis a (in unit of stellar radius, R_*), and the planet's radius R_p (in unit of stellar radius, R_*)—for each filter are given in Table 3. HAT-P-37b's orbit is assumed to be circular.

In order to obtain the best fits for all light curves, we first used a uniform distribution to determine the best value of orbital period P. A uniform distribution between 2.79738 and 2.79748 days was calculated to provide the best value of orbital period of $2.797434 \pm 4 \times 10^{-7}$ days. Next, we investigated the existence of TTVs. We used the ability of `TransitFit` to account for TTV analysis by using the `allow_TTV` function and the best-fit period value from the first procedure was fixed in order to find the midtransit time (T_m) for each epoch. The light curves of HAT-P-37b were phase-folded to each midtransit time at phase of 0.5 with their best-fit models and residuals are shown in Figure 1. The derived planetary parameters for HAT-P-37b are shown in Table 4. The midtransit time (T_m) for each transit event and corresponding epochs (E) are given in Table 6 and discussed in Section 4.

From the analyses, HAT-P-37b has an orbital period of $2.7974341 \pm 4 \times 10^{-7}$ days with the inclination of $i = 87.^{\circ}0 \pm 0.^{\circ}13$ at the star–planet separation of 9.53 ± 0.1 R_*. The obtained parameters are compatible with the values from previous studies: Bakos et al. (2012), Maciejewski et al. (2016), Turner et al. (2017), and Yang et al. (2021). However,

Table 2
The Detrended Photometric Data of HAT-P-37b Transits in This Work

Epoch	BJD	Normalized Flux	Normalized Flux Uncertainty
416	2,456,805.80023	0.999	0.005
	2,456,805.80087	0.999	0.005
	2,456,805.80151	1.000	0.005
	2,456,805.80216	1.001	0.005
	2,456,805.80344	1.002	0.005
	...	...	...
421	2,456,819.81466	1.001	0.003
	2,456,819.81531	0.999	0.003
	2,456,819.81595	1.000	0.003
	2,456,819.81660	0.998	0.003
	2,456,819.81724	0.996	0.003
	...	...	...
436	2,456,861.74956	1.003	0.016
	2,456,861.75085	0.999	0.015
	2,456,861.75149	0.999	0.015
	2,456,861.75213	1.002	0.015
	2,456,861.75277	0.999	0.015
	...	...	...
...	...	...	...

Note. The second-order polynomial detrending functions in `TransitFit` were used. Epoch = 0 is the transit on 2011 March 21. The full table is available in machine-readable form.

(This table is available in its entirety in machine-readable form.)

Table 3
The Initial Parameter Settings and Priors Used to Model the Planetary Parameters with `TransitFit`

Parameter	Priors	Prior Distribution
P (days)	2.797434[a]	Fixed
T_0 (BJD)	$2,455,642.14318 \pm 0.01$	A Gaussian distribution
i (deg)	86.9 ± 1	A Gaussian distribution
a/R_*	9.3 ± 1	A Gaussian distribution
R_p/R_* (B band)	(0.11, 0.15)	Uniform distribution
R_p/R_* (V band)	(0.11, 0.15)	Uniform distribution
R_p/R_* (R band)	(0.11, 0.15)	Uniform distribution
R_p/R_* (Gunn-r)	(0.11, 0.15)	Uniform distribution
R_p/R_* (i' band)	(0.11, 0.15)	Uniform distribution
R_p/R_* (No filter)	(0.11, 0.15)	Uniform distribution
e	0	Fixed

Note. The priors of P, T_0, i, and a/R_* are set as the values in Bakos et al. (2012).

[a] This period value was calculated from the first procedure by uniform distribution.

the R_p/R_* value in B band from the fitting is larger than the value analyzed by Turner et al. (2017; $R_p/R_* = 0.1253 \pm 0.0021$), by about 0.007 ± 0.002.

For the analysis of limb-darkening coefficients (LDCs) of each filter, the `Coupled` fitting mode in `TransitFit` is used. The LDC of each filter is fitted as a free parameter and coupled across wavelengths simultaneously by using the quadratic limb-darkening model and the Limb Darkening Toolkit (LDTk, Husser et al. 2013; Parviainen & Aigrain 2015). The prior of host star information: stellar effective temperature $T_{\rm eff} = 5500 \pm 100$ K, metallicity $[{\rm Fe/H}] = 0.03 \pm 0.1$ (Bonomo et al. 2017), and $\log_g = 4.54 \pm 0.1$ (Stassun et al. 2019)

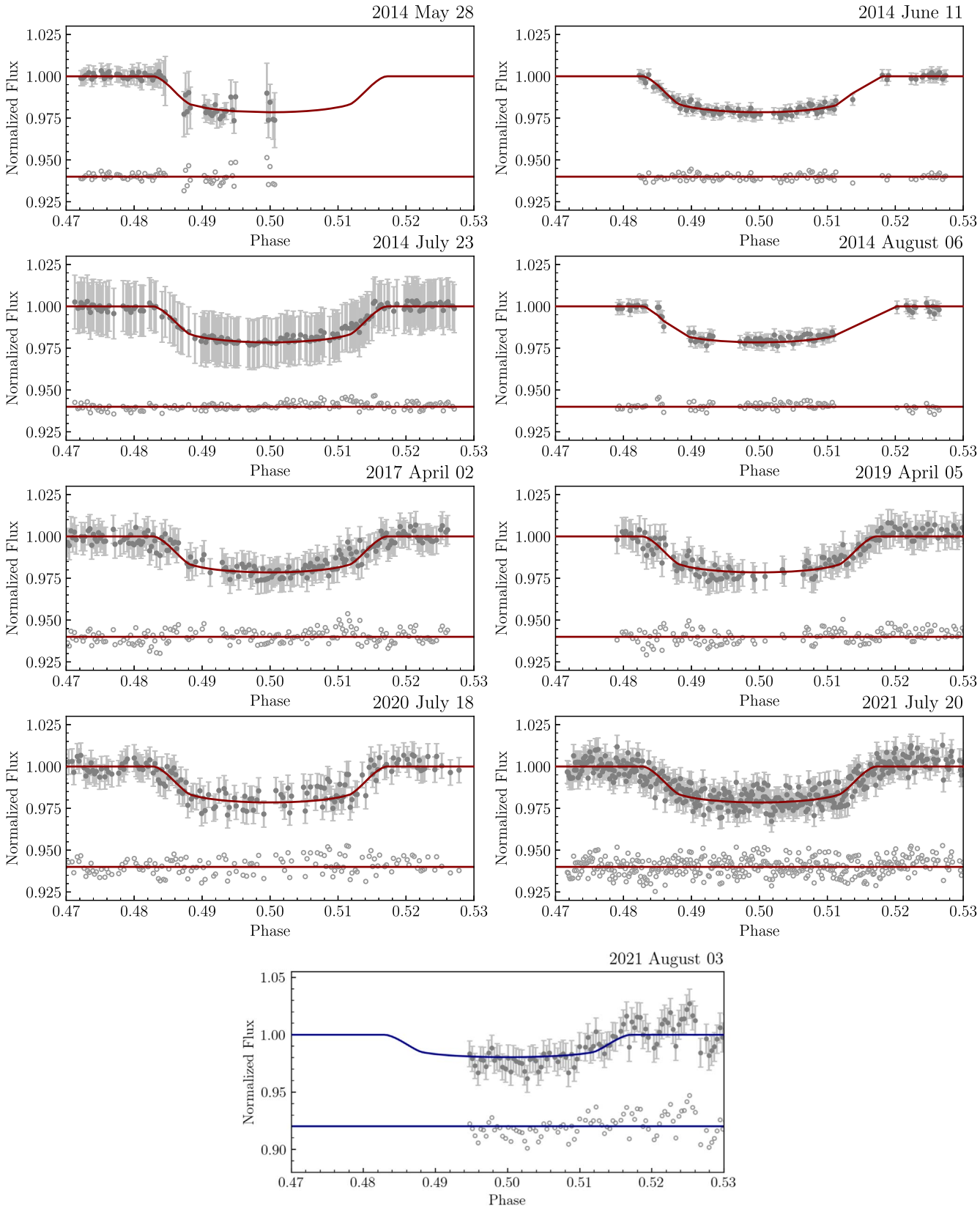

Figure 1. Normalized flux as a function of phased-folded transit light curves of HAT-P-37b from our observations. The red and blue lines represent the best-fitting light curves model for *R* band and *B* band, respectively. The corresponding residuals with offsets 0.94 for *R* band and 0.92 for *B* band are shown below the light curves.

Table 4
The Planetary Parameters from `TransitFit`

Parameter	Value
P (days)	$2.7974341 \pm 4 \times 10^{-7}$
T_0 (BJD)	$2{,}455{,}642.14768 \pm 0.00011$
i (deg)	87.0 ± 0.13
a/R_*	9.53 ± 0.1
R_p/R_* (B band)	0.1316 ± 0.0010
R_p/R_* (V band)	0.1390 ± 0.0006
R_p/R_* (R band)	0.1380 ± 0.0005
R_p/R_* (Gunn-r)	0.1356 ± 0.0007
R_p/R_* (i' band)	0.1374 ± 0.0005
R_p/R_* (No filter)	0.1404 ± 0.0009

are adopted during LDC calculation. The values of LDCs for different filters from the coupled LDC fitting mode are given in Table 5.

4. Transit Timing Analysis

4.1. Timing Variation Models

In order to perform the timing analyses, midtransit times of light curves with full transit coverage in 29 epochs listed in Table 6 are considered. The procedure of timing analyses from Patra et al. (2017) are followed. The midtransit times are fitted by three different models: a linear ephemeris model, an orbital decay model, and an apsidal precession model, using the `emcee` Markov Chain Monte Carlo (MCMC) method (Foreman-Mackey et al. 2013). For each model, 50 chains and 10^5 MCMC steps are computed. As midtransit times are globally obtained from different telescopes for a decade, some data are obtained with precise timing from the GPS clock (e.g., TRT-SRO) while the other data are synchronized via internet clocks (e.g., P60, MTM-500). The timing error from the clock is less than 1 s, which is much smaller than the obtained midtransit time uncertainty. However, the uncertainty of midtransit time could be slightly underestimated from the fitting. In order to correct the underestimation, a smoothing constant, f, is used to calculate the likelihood as

$$\ln \mathcal{L}(D|M) = -\frac{1}{2}\left[\sum_{n}^{N} \ln(2\pi\sigma^2) + \chi^2\right]. \quad (1)$$

The χ^2 function is calculated by

$$\chi^2 = \sum_{n}^{N_{LC}} \frac{(D_n - M_n)^2}{s_n^2}, \quad (2)$$

where D is the observed flux density, M is the modeled flux density and s^2 is the variance of flux measurement,

$$s_n^2 = \sigma_n^2 + f^2 M_n, \quad (3)$$

σ_n is the timing error for the observation.

First, the timing data are fitted with the linear ephemeris model, a constant-period model, as:

$$t(E) = T_{0,l} + E \times P_l, \quad (4)$$

where $T_{0,l}$ and P_l are the reference time and the orbital period of the linear ephemeris model, respectively. E is the epoch number. Epoch = 0 is the transit on 2011 March 21. $t(E)$ is the calculated midtransit time at a given epoch E.

Table 5
Limb-darkening Coefficients of HAT-P-37b from `TransitFit` Using a Coupled LDC Fitting Mode

Filter	u_0	u_1
B	0.441 ± 0.009	0.14 ± 0.01
V	0.448 ± 0.009	0.135 ± 0.009
R	0.445 ± 0.009	0.140 ± 0.009
Gunn-r	0.438 ± 0.009	0.15 ± 0.01
i'	0.446 ± 0.009	0.14 ± 0.01
No Filter	0.439 ± 0.009	0.15 ± 0.01

Table 6
Midtransit Times (T_m) and Timing Residuals ($O - C$) for HAT-P-37b from 17 Transit Light Curves Derived from `TransitFit`

Epoch	$T_m + 2450000$ (BJD_{TDB})	$O - C$ (days)	Data Sources
−9	5616.96681 ± 0.00033	−0.00031	(a)
1	5644.94080 ± 0.00018	−0.00073	(a)
6	5658.92788 ± 0.00014	−0.00085	(a)
176	6134.49375 ± 0.00042	0.00014	(b)
201	6204.43087 ± 0.00069	0.00126	(b)
326	6554.10947 ± 0.00062	−0.0002	(e)
330	6565.30133 ± 0.00028	0.0019	(b)
331	6568.09678 ± 0.00039	−0.00009	(e)
341	6596.07149 ± 0.00080	0.00022	(e)
384	6716.35974 ± 0.00037	−0.00147	(d)
416	6805.87805 ± 0.00176	−0.00126	(f)
421	6819.86407 ± 0.00058	−0.00245	(f)
436	6861.82993 ± 0.00164	0.00181	(f)
441	6875.81335 ± 0.00081	−0.00197	(f)
559	7205.91352 ± 0.00030	0.00022	(c)*
563	7217.10278 ± 0.00039	−0.00027	(e)
588	7287.04016 ± 0.00041	0.00109	(e)
591	7295.43210 ± 0.00033	0.00071	(b)
656	7477.26580 ± 0.00050	0.00079	(d)
788	7846.52635 ± 0.00107	−0.00081	(f)
794	7863.31265 ± 0.00040	0.00085	(d)
814	7919.26183 ± 0.00090	0.00122	(e)
819	7933.24993 ± 0.00068	0.00212	(e)
998	8433.99057 ± 0.00030	0.00092	(e)
1050	8579.45633 ± 0.00095	−0.00022	(f)
1106	8736.11516 ± 0.00037	0.00194	(e)
1218	9049.42530 ± 0.00081	−0.00125	(f)
1349	9415.88838 ± 0.00052	−0.00286	(f)
1354	9429.87531 ± 0.00231	−0.00313	(f)

Note. Epoch = 0 is the transit on 2011 March 21. Data Source: (a) Bakos et al. (2012) (b) Maciejewski et al. (2016) (c) Turner et al. (2017), (d) Wang et al. (2021), (e) Yang et al. (2021) and (f) this study; * : T_m of this epoch was averaged from two transit light curves.

The corner plot of the MCMC posterior probability distribution of the parameters of the constant-period model is shown in Figure A1. The posterior probability distribution provides the best-fit values of $T_{0,l}$ of $2{,}455{,}642.14409^{+0.00046}_{-0.00047}$ (BJD) and P_l of $2.797440^{+0.000001}_{-0.000001}$ days. The reduced chi-square χ^2_{red} of this model is 9.03 with 27 degrees of freedom. Using a new ephemeris, we constructed the $O - C$ diagram, which is the timing residuals from the difference between the timing data and the best fit of the constant-period model as a function of epoch E as shown in Figure 2.

The $O - C$ diagram shows the presence of an inverted parabolic with sinusoidal variation trend. Therefore, the orbital decay and apsidal precession models are adopted in order to

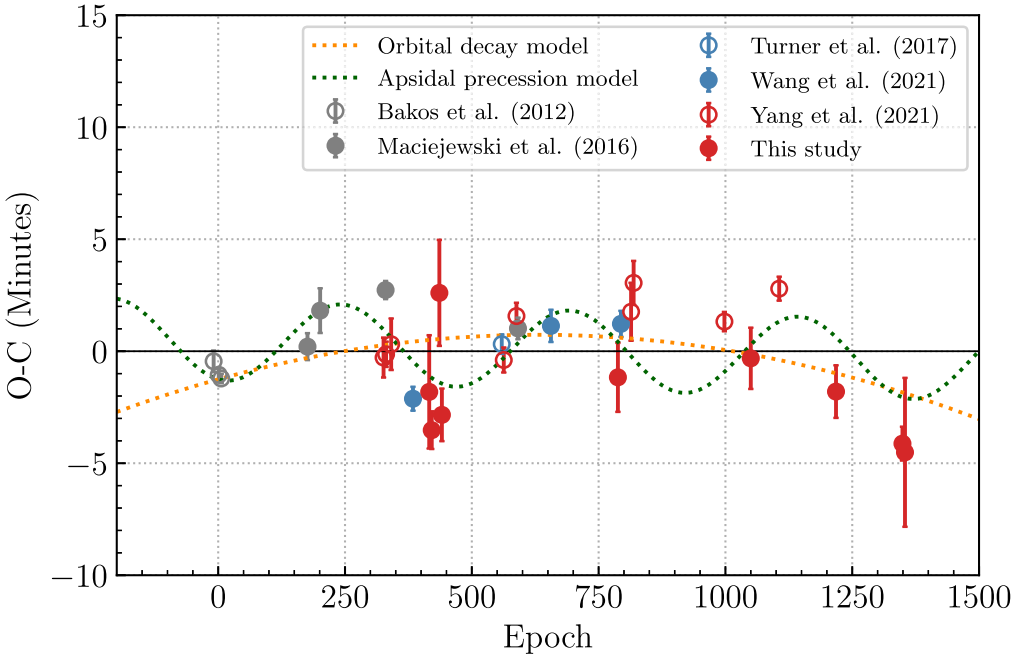

Figure 2. $O-C$ diagram and best-fitting models for HAT-P-37b with the data from Bakos et al. (2012; gray unfilled circles), Maciejewski et al. (2016; gray filled circles), Turner et al. (2017; blue unfilled circles), Wang et al. (2021; blue filled circles), Yang et al. (2021; red unfilled circles), and this work (red filled circles). The orange and green dotted lines present the timing residuals of the orbital decay and apsidal precession models, respectively.

describe the inverted parabolic trend. For the orbital decay model, we assumed that the orbital period is changing at a steady rate as:

$$t(E) = T_{0,d} + E \times P_d + \frac{1}{2}\frac{dP_d}{dE}E^2, \quad (5)$$

where $T_{0,l}$ is a reference time of the orbital decay model, P_d is planetary orbital period of the orbital decay model, and dP_d/dE is the change of orbital in each orbit.

The best-fitting model is shown in Table 7 with the MCMC posterior probability distribution shown in Figure A2. Using the best fitted parameters of this model, the timing residuals as a function of epoch E of the orbital decay model, can be obtained by subtracting with the best-fitting constant-period model is shown in Figure 2. The model shows the change of orbital of $dP_d/dE = -7^{+3}_{-3} \times 10^{-9}$ days/orbit or $-0.08^{+0.03}_{-0.03}$ s yr^{-1}. The $\chi^2_{\rm red}$ of the model is 6.69 with the degree of freedom 26.

The stellar tidal quality factor $Q_\star{}'$ can be expressed as (Maciejewski et al. 2018):

$$Q_\star{}' = -\frac{27}{2}\pi\left(\frac{M_p}{M_\star}\right)\left(\frac{a}{R_\star}\right)^{-5}\left(\frac{dP_d}{dE}\right)^{-1}P, \quad (6)$$

where M_p is the planet mass and $M_\star$ is the stellar mass. The values of M_p and $M_\star$ are taken from Bakos et al. (2012). Using the value of dP_d/dE from the model fitting, we obtained an estimated value of $Q_\star{}' = 250 \pm 10$ which is much smaller than the values supported by theoretical models. Therefore, the orbital decay model is unlikely to be a possible choice here.

The apsidal precession model which can be used to describe the inverted parabolic trend is also adopted. The planet is assumed to have a slight eccentricity e with the argument of pericenter ω that uniformly precesses. The precession model

Table 7
Priors with Uniform Distribution and Best-fitting Parameters from MCMC Transit Timing Analyses

Parameter	Uniform Distribution Priors	Best-fit Values
Constant-period Model		
$P_{orb,l}$ (days)	(2.7, 2.9)	$2.797440^{+0.000001}_{-0.000001}$
$T_{0,l}$ (BJD_{TDB})	(2,455,642.141, 2,455,642.148)	$2{,}455{,}642.14409^{+0.00046}_{-0.00047}$
Orbital Decay Model		
$P_{\rm orb,d}$ (days)	(2.7, 2.9)	$2.797445^{+0.000002}_{-0.000002}$
$T_{0,d}$ (BJD_{TDB})	(2,455,642.141, 2,455,642.148)	$2{,}455{,}642.14322^{+0.00058}_{-0.00057}$
dP/dE (days/orbit)	(−0.5, 0.5)	$-7^{+3}_{-3} \times 10^{-9}$
Apsidal Precession Model		
P_s (days)	(2.7, 2.9)	$2.797440^{+0.000001}_{-0.000001}$
$T_{0,a}$ (BJD_{TDB})	(2,455,642.142, 2,455,642.148)	$2{,}455{,}642.14436^{+0.00042}_{-0.00040}$
e	(0, 0.003)	$0.0013^{+0.0005}_{-0.0004}$
ω_0 (rad)	$(-\pi, \pi)$	$-0.30^{+0.51}_{-0.65}$
$d\omega/dE$ (rad epoch^{-1})	(0, 0.025)	$0.0143^{+0.0009}_{-0.0007}$

from Giménez & Bastero (1995) is used:

$$t(E) = T_{0,a} + E \times P_a - \frac{eP_a}{\pi}\cos\omega(E), \quad (7)$$

where

$$\omega(E) = \omega_0 + \frac{d\omega}{dE}E, \quad (8)$$

$$P_s = P_a\left(1 - \frac{1}{2\pi}\frac{d\omega}{dE}\right). \quad (9)$$

$T_{0,a}$ is the reference time of the apsidal precession model, e is the eccentricity, P_a is the sidereal period, ω is the argument of pericenter, and P_s is the anomalistic period.

In Table 7, the best-fitting parameters from the MCMC posterior probability distribution (Figure A3) are shown. From the result, a nearly circular orbit ($e = 0.0013^{+0.0005}_{-0.0004}$) with $\omega_0 = -0.30^{+0.51}_{-0.65}$ rad and $d\omega/dE = 0.0143^{+0.0009}_{-0.0007}$ rad epoch^{-1} is obtained. The model has $\chi^2_{\rm red} = 4.77$ with 24 degrees of freedom. As a high precession rate, $d\omega/dE$, is obtained; the timing residual in Figure 2 shows a sinusoidal trend instead of a predicted inverted parabolic trend.

From the results of three fitting models, the apsidal procession model provides the highest maximum log likelihood with $\ln \mathcal{L} = 183$. The linear and orbital decay models provide lower maximum log likelihoods of 177 and 180, respectively. Comparing the reduced chi-squared of those three best-fit models, the apsidal procession model also provides the lowest reduced chi-squared value ($\chi^2_{\rm red}$), which can be supported that the timing variation of HAT-P-37b can be favored by the uniform precession model. In order to confirm the argument, the Bayesian information criterion (BIC) of those three models are calculated:

$$\mathrm{BIC} = \chi^2 + k \ln n, \tag{10}$$

where k is the number of free parameters, and n is the number of data points.

From data of 29 epochs ($n = 29$), the values of BIC from linear, orbital decay, and apsidal precession model fits are 250.52, 184.13 and 131.26, respectively. The difference between the BIC value of apsidal precession and orbital decay models is $\Delta\mathrm{BIC} = 52.87$. Therefore, the apsidal precession model is favorable for the timing data fitting.

However, the apsidal precession model fitting shows sinusoidal variation with transit time data. This variation might be affected by the light-time effect (LiTE) due to the third component in the HAT-P-37 system. Therefore, the timing variation due to a third body in the system is analyzed in the rest of this section.

4.2. The Frequency Analysis of TTVs

In order to investigate the sinusoidal of TTVs on HAT-P-37b data, we use the generalized Lomb–Scargle periodogram (GLS; Zechmeister & Kürster 2009) in the `PyAstronomy`[14] routine (Czesla et al. 2019) to search for periodicity in the timing residual ($O - C$) data given in Table 7. The false-alarm probability (FAP) is calculated in order to provide the probability of peak detection from the highest power peak. The result of GLS is shown in the periodogram of the power spectrum as a function of frequency in Figure 3. In the periodogram, the highest power peak = 0.574 at a frequency of 0.0023 ± 0.0001 cycle/period (epoch) calculated from FAP of 0.02 % is found. However, this FAP level consists of noise and no significant periodicity. The FAP levels of 0.5%, 0.1%, and 0.01% are presented.

Nevertheless, the frequency of the highest power peak is tested by assuming TTVs with a sinusoidal variability. We apply the procedure described in von Essen et al. (2019). The timing residuals were fitted through a fitting function as:

$$\mathrm{TTVs}(E) = A_{\rm TTVs} \sin(2\pi f E - \phi), \tag{11}$$

where $A_{\rm TTVs}$ is the amplitude (minutes) of the timing residuals, f is the frequency on the highest peak of power periodogram, and ϕ is the phase.

From the fitting, $A_{\rm TTVs} = 1.74 \pm 0.17$ minutes and $\phi = 2.2 \pm 0.08$ with the best fitted $\chi^2_{\rm red} = 4.39$ and BIC = 125.25 are obtained. The timing residuals with the best fit of sinusoidal variability is plotted in Figure 3. The reduced chi-squared and BIC values of the sinusoidal model are lower than the values from the apsidal precession model. Therefore, there is a possibility of having an additional exoplanet in the system.

An additional exoplanet that has an orbital period near the the first-order resonance of HAT-P-37b with a coplanar orbit is assumed. With a first-order mean-motion resonance, j:j-1, the perturber planet mass can be calculated from the Lithwick et al. (2012) equation:

$$V = P \frac{\mu'}{\pi j^{2/3} (j-1)^{1/3} \Delta} \left(-f - \frac{3}{2} \frac{Z^*_{\rm free}}{\Delta} \right), \tag{12}$$

where V is the amplitude of transit time variation. For our case $V = 1.74$ minutes. P is period of HAT-P-37b, μ' is the outer planet mass, Δ is the normalized distance to resonance, f is sums of Laplace coefficients with order-unity values and $Z^*_{\rm free}$ is the dynamical quantity that controls the TTV signal (more explanation given in Lithwick et al. 2012).

From the calculation, in the case of 1:2 mean-motion resonance, the mass of the additional planet could be as small as $0.0002 M_{\rm Jup}$ or $0.06 M_\oplus$ with a period of 5.58 days. The perturber mass is lighter than the Earth. Assuming the planet is a rocky planet with the Earth's density, it has a radius of $0.4\ R_\oplus$. If the planet transit the host star, it will produce a transit depth of 1.75×10^{-5}, which cannot be detected by the light-curve precision in this work.

4.3. Upper-mass Limit for an Additional Planet

From Section 4.2, an additional planet orbiting near 1:2 mean-motion resonance of HAT-P-37b is investigated. In this section the upper-mass limit for an additional planet near HAT-P-37b is found from the timing variation. We follow the method given in Awiphan et al. (2016) to search for the upper-mass limit of the second planet. First, we assumed that two planets are coplanar and have circular orbits. The unstable region is calculated from the mutual Hill sphere between HAT-P-37b and the perturber by Fabrycky et al. (2012);

$$r_H = \frac{a_{\rm in} + a_{\rm out}}{2} \left(\frac{M_{\rm in} + M_{\rm out}}{3 M_\star} \right)^{1/3}, \tag{13}$$

where $a_{\rm in}$ and $a_{\rm out}$ are the semimajor axis of the inner and outer planets, respectively. The boundary of the stable orbit is when the separation of the planets' semimajor axes ($a_{\rm out} - a_{\rm in}$) is larger than $2\sqrt{3}$ of the mutual Hill sphere. The region of unstable orbits is shown by the black shaded area in Figure 4.

We use the `TTVFaster`[15] by Deck & Agol (2016), a package for dynamical analysis that is accurate to first order in orbital eccentricity to search for TTV signals of secondary planets. The period ratio between the perturber planet and

[14] PyAstronomy: https://github.com/sczesla/PyAstronomy.

[15] TTVFaster: https://github.com/ericagol/TTVFaster.

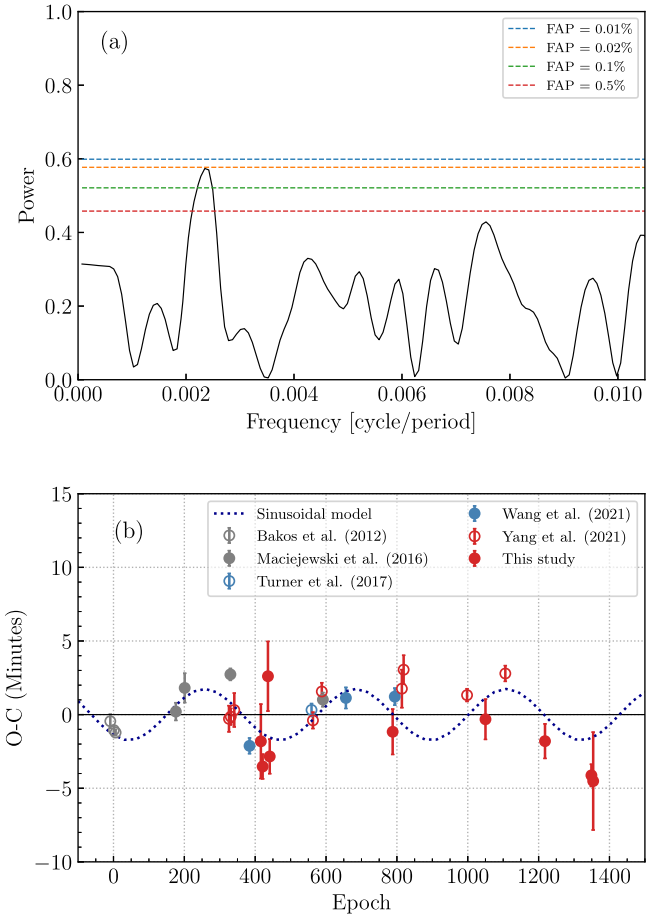

Figure 3. Searching for possible periodicity of TTVs of HAT-P-37b (a) GLS periodogram for timing residuals from Table 6. The dashed lines indicate the FAP levels. (b) $O-C$ diagram and the best fit of sinusoidal variability from the frequency of the highest power peak, FAP = 0.02% (blue dotted line).

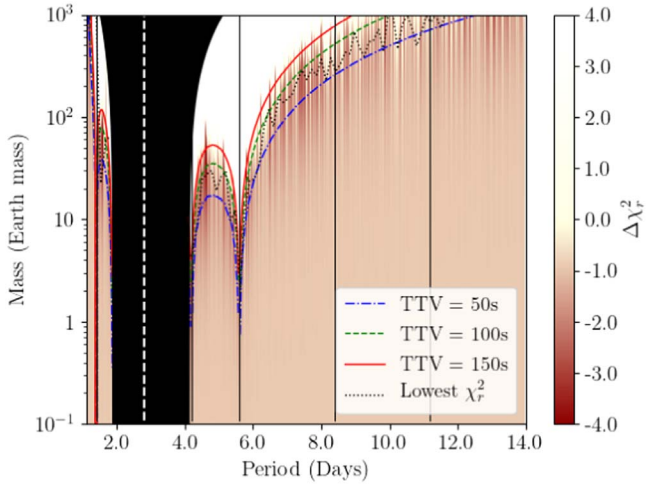

Figure 4. Upper-mass limit of the perturbing planet in the HAT-P-37 system. The upper-mass limit for TTV amplitudes of 50, 100, and 150 s are shown in blue dashed–dotted, green dashed, and red solid lines, respectively. The best $\Delta\chi^2_{\rm red}$ within a 0.05 period ratio bin is presented by the black dotted line. The contours represent the best $\Delta\chi^2_{\rm red}$ between the best TTV model and the best linear model. The unstable orbit region is shown by the black shaded region. The right vertical dashed line displays the orbital period of HAT-P-37b. The black vertical lines show 2:1, 3:2, 1:2, 1:3, and 1:4 orbital period resonance from left to right, respectively.

HAT-P-37b between 0.3 and 5.0 with 0.01 steps is set with the mass range between 10^{-1} and 10^3 Earth mass in logarithmic scale. From the amplitude signal 104.4 s on the $O-C$ diagram in Section 4.2, we calculate the upper-mass limits corresponding to TTV signal amplitudes of 50, 100, and 150 s shown in Figure 4.

Finally, using the comparison between $\chi^2_{\rm red}$ values of the best linear fitting model, a single-planet model, and $\chi^2_{\rm red}$ of the signal from the two planets model by `TTVFaster` as:

$$\Delta\chi^2_{\rm red} = \chi^2_{\rm red} - \chi^2_{{\rm red},l}, \tag{14}$$

where $\chi^2_{\rm red}$ is the best fitting of second planet model (TTV model) at a given mass and period and $\chi^2_{{\rm red},l}$ is the best fitting of the single-planet model. $\chi^2_{{\rm red},l} = 9.03$ is obtained from Section 4.1. The $\Delta\chi^2_{\rm red}$ is shown as a function of perturber mass and period in Figure 4. The regions of negative values of $\Delta\chi^2_{\rm red}$ are near the 100 s TTV amplitude as predicted. From the result, we can conclude that there is no Saturn-mass planet within 1:2 orbital period resonance.

5. HAT-P-37b Atmosphere

The investigation of variations in the transit depth with wavelength of HAT-P-37b was discussed by Turner et al. (2017). They found that HAT-P-37b shows a small transit depth in the B filter may be caused by TiO/VO absorption. From this investigation, the study of HAT-P-37b transmission spectrum is considered.

From R_p/R_* values from different filters obtained from Section 3, the broadband transmission spectrum of HAT-P-37b is shown in Figure 5. The PLanetary Atmospheric Transmission for Observer Noobs (`PLATON`[16]; Zhang et al. 2019) is used to model and retrieves atmospheric characteristics of the transmission spectrum. For a `PLATON` retrieval run, 1000 live points are performed by the nested sampling method with the priors as in Table 8.

The transit depths of five filters: B, V, R, r', and i' bands, with wavelength coverage between 390 and 779 nm are obtained in Section 3. From the fitting, the HAT-P-37b radius at 100,000 Pa of 1.11 $R_{\rm Jup}$ and mass of 1.17 $M_{\rm Jup}$ are obtained with the host stellar radius of 0.86 $R_\odot$ (Table 8 and Figure B1). The model shows the temperature of the HAT-P-37b atmosphere with the isothermal model of 1800 K. However, the model provides the χ^2 value 42 with a large discrepancy in B-filter data, which is obtained from two transits from Turner et al. (2017) and a partial transit from the TRT-SBO. As the model cannot fit the depth in B filter, the depth is excluded from further analysis.

Another model without the depth in B-fitting is fitted with `PLATON`. Four transit depth data in V, R, r', and i' filters with wavelength range 501–779 nm are modeled. The best-fitting results are shown in Table 8 and Figure B2. The result provides a cooler atmospheric temperature of 1100 K with χ^2 of 18. However, the cloudy model, i.e., a model with a constant transit depth, of the data without the depth in B filter provides the planet–star radius ratio of 0.137 and χ^2 of 16, which is lower than the chi-squared values of both `PLATON` fitting models. Therefore, there is a possibility that thick clouds cover the HAT-P-37b atmosphere.

[16] PLATON: https://github.com/ideasrule/platon.

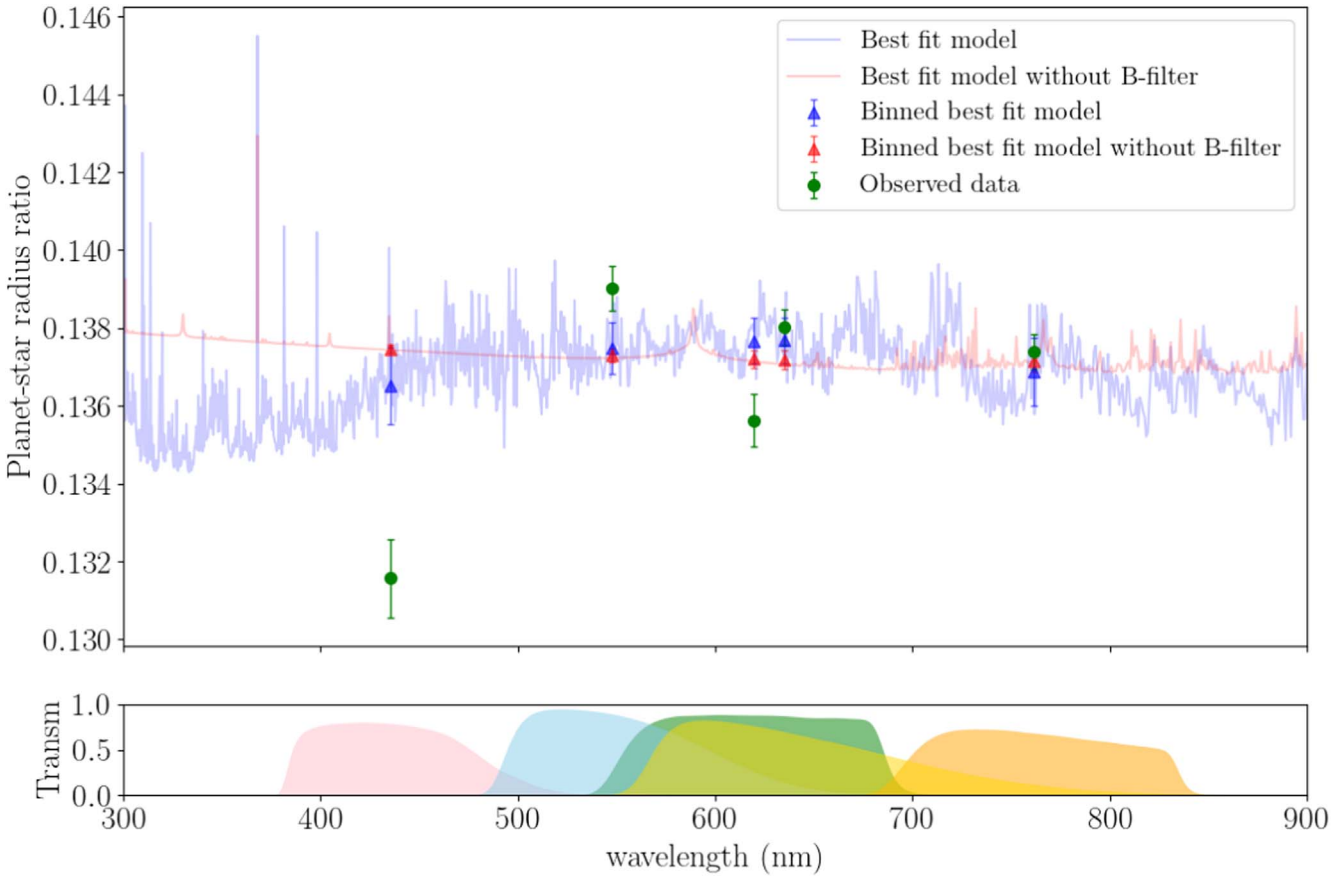

Figure 5. The best-fit transmission spectrum of HAT-P-37b with synthetic models generated from PLATON retrieval (top) and the bandpass filters: B, V, R, r, and i band (from left to right; bottom).

Table 8
The Priors and Prior Distribution Used for PLATON Retrieval and the Best-fit Parameters of Each Wavelength Range Analysis from the Retrieval

Parameter	Priors	Prior Distribution	Wavelength Range 390–779 nm	Wavelength Range 501–779 nm
R_s ($R_\odot$)	0.87 ± 0.06	Gaussian distribution	$0.86^{+0.02}_{-0.02}$	$0.86^{+0.02}_{-0.02}$
M_p ($M_{\rm Jup}$)	1.169 ± 0.1	Gaussian distribution	$1.17^{+0.04}_{-0.04}$	$1.18^{+0.04}_{-0.04}$
R_p ($R_{\rm Jup}$)	(1.06, 1.30)	Uniform distribution	$1.11^{+0.03}_{-0.03}$	$1.15^{+0.03}_{-0.03}$
T (K)	(635, 1900)	Uniform distribution	1900^{+400}_{-500}	1100^{+400}_{-400}
$\log_{\rm Scattering\ Factor}$	(0, 2)	Uniform distribution	$0.9^{+0.7}_{-0.6}$	$1.1^{+0.7}_{-0.7}$
$\log_{Z/Z_\odot}$	(−0.8, 1.6)	Uniform distribution	$0.6^{+0.8}_{-0.8}$	$0.3^{+0.8}_{-0.8}$
C/O ratio	0.3	Fixed	0.3	0.3
Error multiple	(0.5, 5)	Uniform distribution	$3.6^{+0.8}_{-0.9}$	$1.8^{+1.3}_{-0.9}$

Note. The priors of R_s, M_p, and R_p are set as the values from Bakos et al. (2012).

6. Conclusions

In this work, the photometric observations and studies of a hot Jupiter HAT-P-37b are performed. Nine transit light curves are obtained from three telescopes: the 60 inch telescope at Palomar Observatory, the 50 cm Maksutov telescope at the CrAO, Crimea, and the 0.7 m Thai Robotic Telescope at Sierra Remote Observatories. The observational data are combined with 21 published light curves. Using the TransitFit, the HAT-P-37b parameters and the midtransit times are obtained. From the fitting, the planet has an orbital period of $2.7974341 \pm 4 \times 10^{-7}$ days, the inclination of $i = 87\overset{\circ}{.}0 \pm 0\overset{\circ}{.}13$ and the star–planet separation of 9.53 ± 0.1 R_* which are consistent with previous works. The planet–star radius ratios in five wave bands: B, V, R, r', and i', are obtained. Nevertheless, the fitted transit depth in B band from this study is larger than the value analyzed by Turner et al. (2017).

From the fitting, 29 midtransit times are obtained. The $O - C$ diagram of the HAT-P-37b midtransit time shows an inverted parabola with a sinusoidal variation trend. Therefore, three timing variation models: a linear ephemeris model, an orbital decay model, and an apsidal precession model are used to analyze the variation. The stellar tidal quality factor $Q_\star{}'$ is determined to be 250 ± 10 which is far too small and inconsistent with theoretical estimation. The apsidal precession is favorable for the timing data fitting with $d\omega/dE = 0.0143^{+0.0009}_{-0.0007}$ rad epoch^{-1}, maximum log likelihood of

$\ln \mathcal{L} = 183$ and $\chi^2_{\rm red}$ of 4.77. However, due to the large value of $d\omega/dE$, the model shows a sinusoidal variation on transit time data which might be explained by LiTE of the third body in the system. Therefore, the timing residual $(O-C)$ data were considered by frequency analysis and sinusoidal variability model fitting. From the analysis, the TTV amplitude signal of 1.74 ± 0.17 minutes is obtained. If the third-body orbit is at the 1:2 mean-motion resonance, its mass can be as small as $0.0002 M_{\rm Jup}$ or $0.06 M_{\oplus}$. The upper-mass limit for the perturber planet in the HAT-P-37 system is calculated using the `TTVFaster` package. The results show that there is no nearby ($P < 3$ days) planet with mass heavier than Saturn around HAT-P-37b. The mutual Hill sphere regions between the orbital period of 1.9–4.2 days represents the excluding of the presence of a nearby planet.

For the transmission spectroscopy analysis of HAT-P-37b, the transit depths of five filters B, V, R, r', and i' bands with wavelength range between 390 and 779 nm are modeled by the `PLATON` fitting model. The model shows the temperature of HAT-P-37b's atmosphere with the isothermal temperature model of 1800 K with a large χ^2 value ($\chi^2 = 42$) due to a large discrepancy in the B-filter data. Therefore, the model without the transit depth in B filter is considered. The model provides a cooler atmospheric temperature of 1100 K with $\chi^2 = 18$. However, this chi-square value is still larger than the value of the constant transit depth mode ($\chi^2 = 16$), which can refer to a cloudy atmospheric model.

Although a small additional planet and a cloudy atmosphere model of HAT-P-37b can be concluded from the analyses in this work, additional high-precision observation data in both transit timing and transit depth, especially in the blue wave band, are needed before the perturber and the atmospheric model can be confirmed.

We thank the anonymous referee for good comments and suggestions that helped to improve the quality of this paper. This work is supported by a grant from the Ministry of Science and Technology (MOST), Taiwan. The grant numbers are MOST 109-2112-M-007-007 and MOST 110-2112-M-007-035. There are two nights of observational data based on observations made with the Thai Robotic Telescopes, which are operated by the National Astronomical Research Institute of Thailand (Public Organization). This work is also partially supported by a National Astronomical Research Institute of Thailand (Public Organization) research grant. We thank all the authors of previous HAT-P-37b papers for kindly providing their observational data to make this work possible.

Facilities: P60 (Palomar Observatory), MTM-500 (CrAO) and 0.7 m (TRT-SRO).

Software: `sextractor` (Bertin & Arnouts 1996), `Astrometry.net` (Lang et al. 2010), `TransitFit` (Hayes et al. 2021), `TTVFaster` (Deck & Agol 2016) and `PLATON` (Zhang et al. 2019).

Appendix A
Posterior Probability Distribution for Three TTV Model MCMC Fitting Parameters

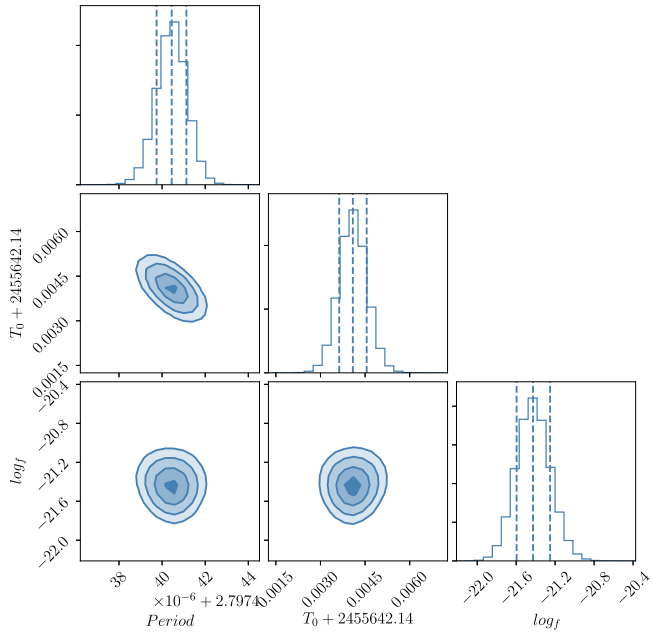

Figure A1. Posterior probability distribution of the constant-period model MCMC fitting parameters.

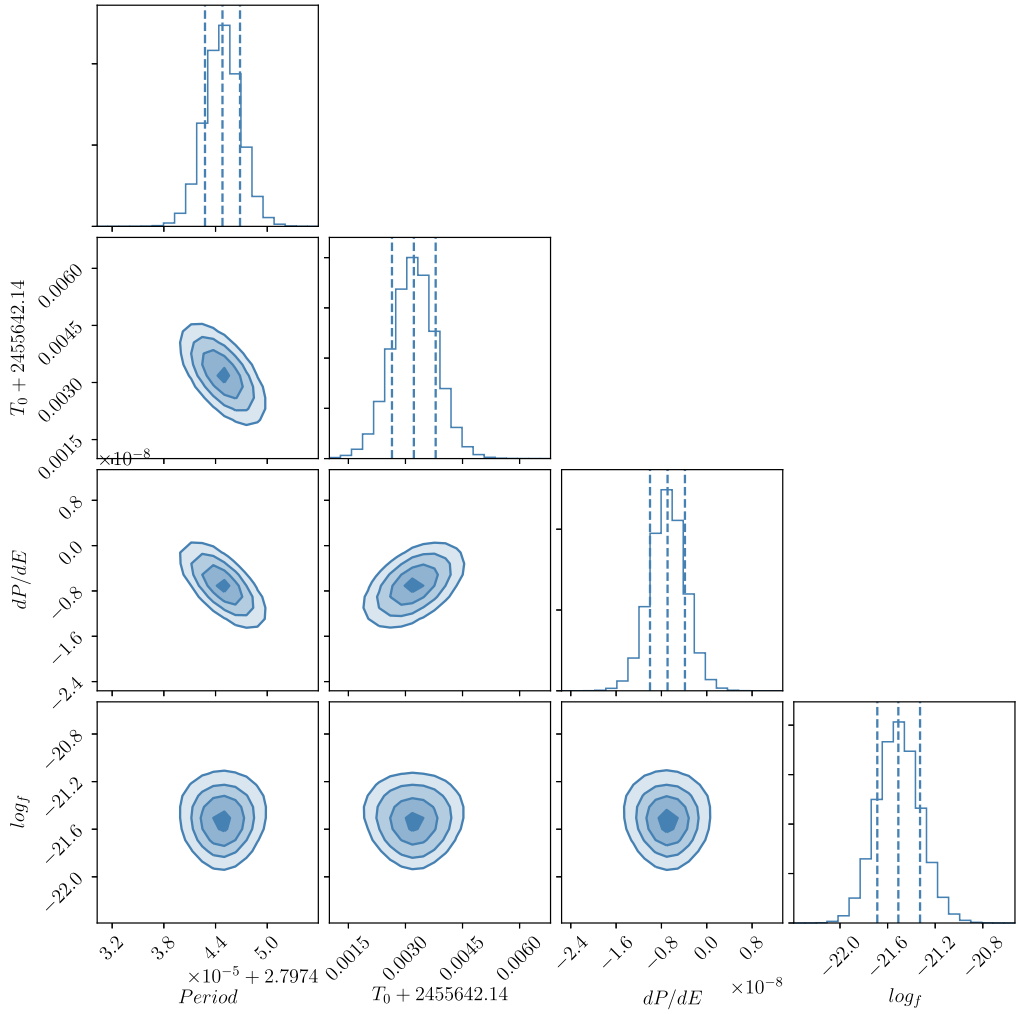

Figure A2. Posterior probability distribution of the orbital decay model MCMC fitting parameters.

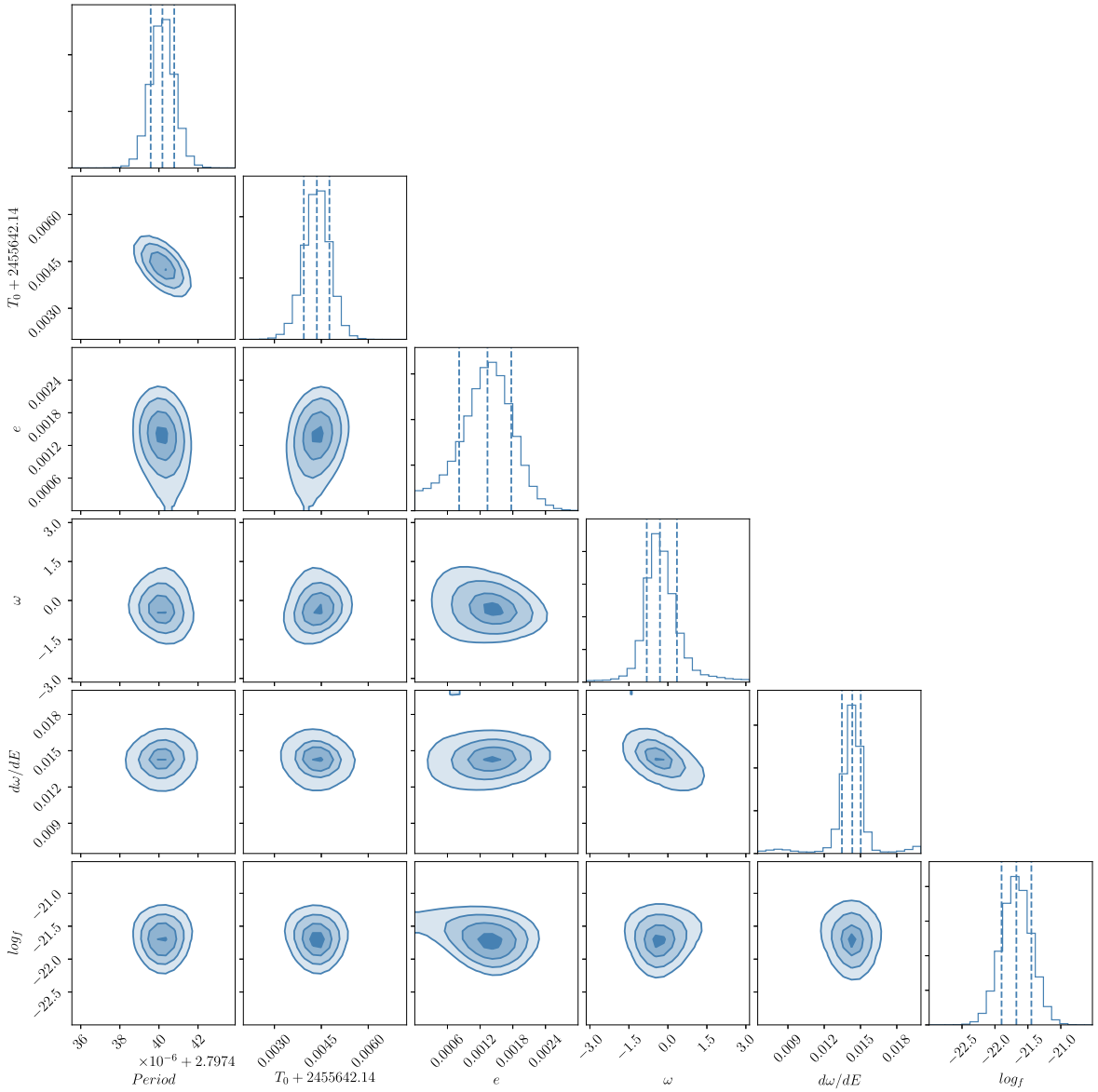

Figure A3. Posterior probability distribution of the apsidal precession model MCMC fitting parameters.

Appendix B
Posterior Probability Distributions from PLATON for HAT-P-37b Transmission Spectrum Study

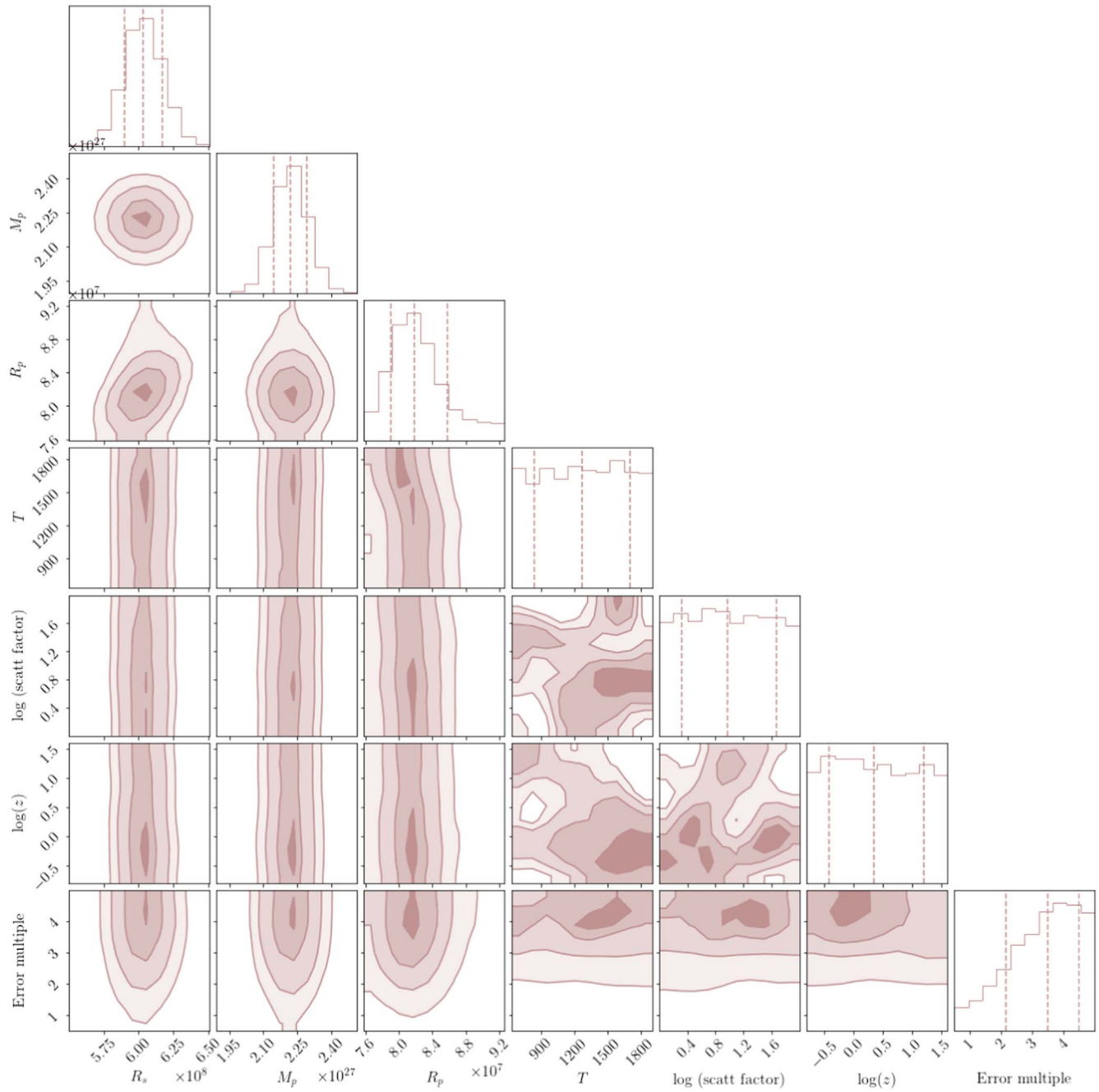

Figure B1. Posterior probability distributions from PLATON retrieval for HAT-P-37b of wavelength range 390–779 nm (including *B* filter).

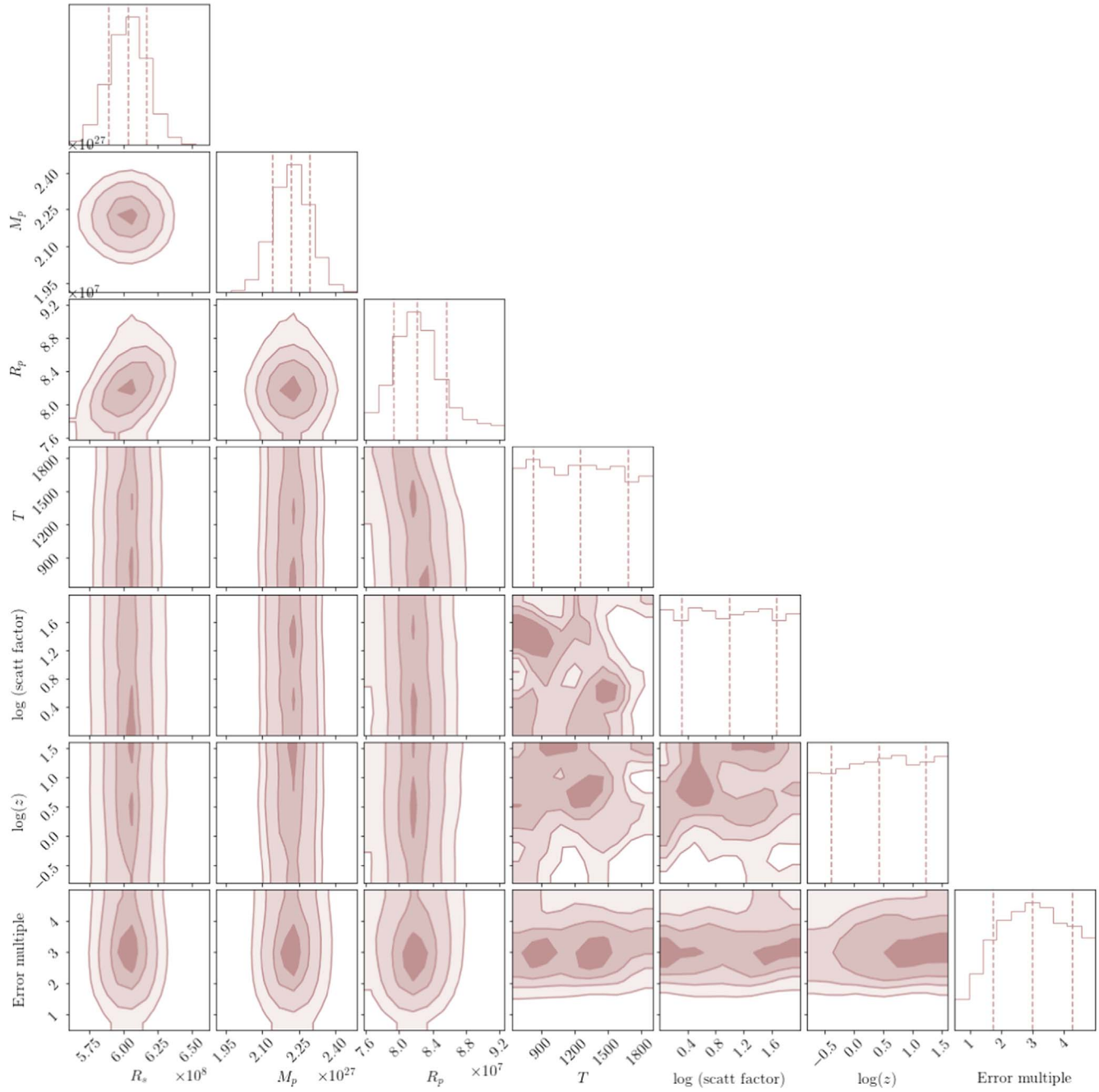

Figure B2. Posterior probability distributions from PLATON retrieval for HAT-P-37b of wavelength range 501–779 nm (without *B* filter).

ORCID iDs

Napaporn A-thano https://orcid.org/0000-0001-7234-7167
Ing-Guey Jiang https://orcid.org/0000-0001-7359-3300
Supachai Awiphan https://orcid.org/0000-0003-3251-3583
Devesh P. Sariya https://orcid.org/0000-0001-8452-7667
A. A. Shlyapnikov https://orcid.org/0000-0002-2752-2429
Mark A. Gorbachev https://orcid.org/0000-0001-5731-9264
Vineet Kumar Mannaday https://orcid.org/0000-0002-0638-950X
Parijat Thakur https://orcid.org/0000-0001-5958-0562

References

Agol, E., Steffen, J., Sari, R., & Clarkson, W. 2005, MNRAS, 359, 567
Awiphan, S., Kerins, E., Pichadee, S., et al. 2016, MNRAS, 463, 2574
Bakos, G., Noyes, R. W., Kovács, G., et al. 2004, PASP, 116, 266
Bakos, G. Á., Hartman, J. D., Bhatti, W., et al. 2021, AJ, 162, 7
Bakos, G. Á., Hartman, J. D., Torres, G., et al. 2012, AJ, 144, 19
Bertin, E., & Arnouts, S. 1996, A&AS, 117, 393
Bonomo, A. S., Desidera, S., Benatti, S., et al. 2017, A&A, 602, A107
Borucki, W. J., Koch, D., Basri, G., et al. 2010, Sci, 327, 977
Charbonneau, D., Brown, T. M., Noyes, R. W., & Gilliland, R. L. 2002, ApJ, 568, 377

Czesla, S., Schröter, S., Schneider, C. P., et al. 2019, PyA: Python astronomy-related packages, Astronomical Source Code Library, ascl:1906.010
Deck, K. M., & Agol, E. 2016, ApJ, 821, 96
Fabrycky, D. C., Ford, E. B., Steffen, J. H., et al. 2012, ApJ, 750, 114
Foreman-Mackey, D., Hogg, D. W., Lang, D., & Goodman, J. 2013, PASP, 125, 306
Fulton, B. J., Shporer, A., Winn, J. N., et al. 2011, AJ, 142, 84
Giménez, A., & Bastero, M. 1995, Ap&SS, 226, 99
Hayes, J. J. C., Kerins, E., Morgan, J. S., et al. 2021, arXiv:2103.12139
Holman, M. J., & Murray, N. W. 2005, Sci, 307, 1288
Husser, T. O., Wende-von Berg, S., Dreizler, S., et al. 2013, A&A, 553, A6
Jiang, I.-G., Yeh, L.-C., Thakur, P., et al. 2013, AJ, 145, 68
Kanodia, S., & Wright, J. 2018, RNAAS, 2, 4
Kreidberg, L. 2015, PASP, 127, 1161
Lang, D., Hogg, D. W., Mierle, K., Blanton, M., & Roweis, S. 2010, AJ, 139, 1782
Lithwick, Y., Xie, J., & Wu, Y. 2012, ApJ, 761, 122
Maciejewski, G., Dimitrov, D., Mancini, L., et al. 2016, AcA, 66, 55
Maciejewski, G., Dimitrov, D., Neuhäuser, R., et al. 2010, MNRAS, 407, 2625
Maciejewski, G., Fernández, M., Aceituno, F., et al. 2018, AcA, 68, 371
Mannaday, V. K., Thakur, P., Jiang, I.-G., et al. 2020, AJ, 160, 47
Parviainen, H., & Aigrain, S. 2015, MNRAS, 453, 3821
Patra, K. C., Winn, J. N., Holman, M. J., et al. 2017, AJ, 154, 4
Ricker, G. R., Winn, J. N., Vanderspek, R., et al. 2014, Proc. SPIE, 9143, 914320
Seager, S., & Sasselov, D. D. 2000, ApJ, 537, 916
Sing, D. K., Fortney, J. J., Nikolov, N., et al. 2016, Natur, 529, 59
Southworth, J., Dominik, M., Jørgensen, U. G., et al. 2019, MNRAS, 490, 4230
Speagle, J. S. 2020, MNRAS, 493, 3132
Stassun, K. G., Oelkers, R. J., Paegert, M., et al. 2019, AJ, 158, 138
Turner, J. D., Leiter, R. M., Biddle, L. I., et al. 2017, MNRAS, 472, 3871
von Essen, C., Wedemeyer, S., Sosa, M. S., et al. 2019, A&A, 628, A116
Wang, X.-Y., Wang, Y.-H., Wang, S., et al. 2021, ApJS, 255, 15
Yang, J.-M., Wang, X.-Y., Li, K., & Liu, Y. 2021, PASJ, 73, 1010
Zechmeister, M., & Kürster, M. 2009, A&A, 496, 577
Zhang, M., Chachan, Y., Kempton, E. M. R., & Knutson, H. A. 2019, PASP, 131, 034501